Investigation of the thermal efficiency of a staggered elliptic-tube heat exchanger for aeroengine applications

K. Kritikos, C. Albanakis, D. Missirlis, Z. Vlahostergios, A. Goulas, P. Storm

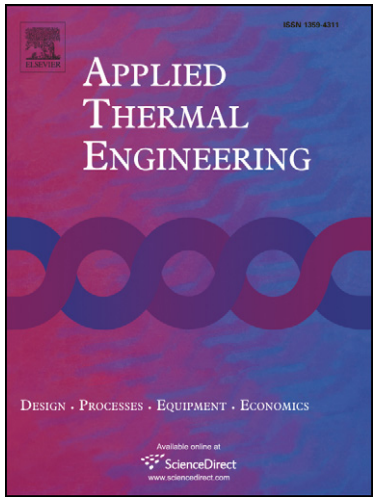

Investigation of the thermal efficiency of a staggered elliptic-tube heat exchanger for aeroengine applications

K. Kritikos, C. Albanakis, D. Missirlis, Z. Vlahostergios, A. Goulas, P. Storm

PII: S1359-4311(09)00231-2
DOI: 10.1016/j.applthermaleng.2009.07.013
Reference: ATE 2865

To appear in: *Applied Thermal Engineering*

Received Date: 14 May 2009
Accepted Date: 23 July 2009

Please cite this article as: K. Kritikos, C. Albanakis, D. Missirlis, Z. Vlahostergios, A. Goulas, P. Storm, Investigation of the thermal efficiency of a staggered elliptic-tube heat exchanger for aeroengine applications, *Applied Thermal Engineering* (2009), doi: 10.1016/j.applthermaleng.2009.07.013

Investigation of the thermal efficiency of a staggered elliptic-tube heat exchanger for aeroengine applications

K. Kritikos [a], C. Albanakis [a], D. Missirlis [a*], Z.Vlahostergios [a], A.Goulas [a], P. Storm [b]

[a] *Laboratory of Fluid Mechanics and Turbomachinery, Department of Mechanical Engineering, Aristotle University of Thessaloniki, Thessaloniki 54 124, Greece*

[b] *MTU Aero Engines GmbH, Munich, Germany*

[*]Corresponding author. E-mail address: misirlis@eng.auth.gr (D. Missirlis).

Abstract

In this paper, a numerical investigation of the thermal performance of a heat exchanger designed for aero engine applications is performed with the use of computational fluid dynamics (CFD). For this purpose, the exact geometry of the heat exchanger was modeled, and additionally the use of a porous medium methodology was adopted. For the latter the behaviour of the heat exchanger was described by experimentally derived pressure drop and heat transfer laws. The heat transfer performance of the heat exchanger can be described by the Nusselt number of the flow and the temperature distribution inside the heat exchanger. At the present work the CFD results regarding the overall and local Nusselt numbers and the temperature distributions were compared to available experimental data and were found to be in agreement. Thus, both approaches could be used for the detailed investigation of the thermal performance of the heat exchanger so that useful conclusions could be derived.

Keywords: heat exchanger, heat transfer, Nusselt number, porous medium, pressure drop.

Nomenclature

A	heat exchange area per unit of volume	T	temperature
b	small semi-axis of the elliptic tube	u	x-velocity component
C_p	specific heat under constant pressure	$\tilde{u}$	Favre averaged velocity
		u_i	velocity component
C_v	specific heat under constant volume	U	velocity magnitude
		v	y-velocity component
D	cylinder diameter	V	flow velocity component matrix
D_h	hydraulic diameter	w	z-velocity component
D'	1st order pressure drop coefficient matrix		
$D'_{i,j}$ $_{i,j=x,y,z}$	diagonal coefficients in the 1st order pressure drop coefficient matrix	*subscripts*	
E	internal energy	b	bulk
e_0	total energy	f	fluid
F'	2nd order pressure drop coefficient matrix	in	inlet
$F'_{i,j}$ $_{i,j=x,y,z}$	diagonal coefficients in the 2nd order pressure drop coefficient matrix	local	local value
		m	mean
f	frequency	max	maximum
h	heat transfer coefficient	out	outlet
$\tilde{k}$	turbulence kinetic energy	w	wall
L	characteristic length	∞	free stream
Nu	Nusselt number		
p	pressure	*Greek symbols*	
$\overline{p}$	Reynolds averaged pressure		
Pr	Prandtl number	δ_{ij}	Kronecker delta
$\dot{q}$	heat flux per unit volume	$\tilde{\varepsilon}^*$	Isotropic part of dissipation rate
$\dot{q}_w$	wall heat flux	κ	thermal conductivity
Re	Reynolds number	μ	viscosity
S_M	pressure drop matrix	ν	kinematic viscosity
St	Strouhal number	ρ	density

1. Introduction

Nowadays, the pressure for reducing fuel consumption and pollutant emissions and the development of environmentally friendlier aero engines is significantly increased. Towards this direction, aeronautic engineers are obliged to exploit every aspect of the

operation of an aero engine. Focused on this goal, MTU Aero Engines has developed the concept of the Intercooled Recuperative Aero engine (IRA), which uses a less conventional but more efficient thermodynamic cycle, Boggia [1].

The concept of the recuperative engine is shown in **Fig 1**. As it can be seen, a number of heat exchangers are installed inside the exhaust nozzle of an aero engine, immediately downstream of the turbine exit. The main target of the heat exchangers is the exploitation of the thermal energy of the turbine exhaust gas in order to pre-heat the compressor outlet air before combustion and thus to decrease fuel consumption and pollutant emissions.

Fig. 1 The IRA aero engine

Since the heat exchangers are a critical part of this technology, the optimization of their performance can maximize its benefits. For this reason, experimental and numerical methods can be introduced. The performance of the heat exchanger was investigated experimentally in the work of Albanakis et al. [2]. However, in their work it was not possible to proceed to detailed measurements inside the heat exchanger core in order to investigate the local heat transfer performance and towards this direction numerical methods can be used.

Such an effort is presented in this work where computational tools are developed in order to provide a detailed view of the flow field and the heat transfer taking place inside the heat exchanger core. The numerical investigation is performed with two

approaches: at first, with the use of computational fluid dynamics (CFD), where the exact geometry of the heat exchanger was modeled and second, with the use of a porous medium methodology where the behaviour of the heat exchanger was described by experimentally derived pressure drop and heat transfer laws.

The first attempts to investigate the behaviour of this heat exchanger have been presented in the work of Missirlis et al. [3,4] who presented an experimental and numerical study of the heat exchanger. In their work the heat exchanger was treated as a porous medium with predefined pressure drop derived from detailed experimental measurements. Additionally, Yakinthos et al. [5,6], presented an optimization effort of the overall heat exchanger installation with the use of the previously developed porous medium model together with a wide range of experimental measurements. In these works, the main parameter under consideration was the reduction of pressure losses since the experimental measurements were corresponding to isothermal flow conditions. Thus, the heat transfer efficiency of this heat exchanger has not been extensively studied yet. The latter is the main target of the present work.

The investigation of the flow field and the heat transfer in tube bundle heat exchangers has been presented in detail in various works of international literature.

Studies involving flow-over-tube bundle heat exchangers, consisting of either elliptical or circular tubes, have been the subject of numerous experimental and numerical works. An extended experimental work aiming to study the pressure losses and the heat transfer of flow through a tube bundle heat exchanger has been performed by Zukauskas and

Ulinskas [7]. After examining many different geometrical settings and parameters, they suggested correlations for heat transfer with the Reynolds and Prandtl number and for the pressure drop with the velocity and the geometrical characteristics.

Furthermore, Ahmad [8] did a bibliographic work and a numerical effort to present the dependence of the drag coefficient and thermal field with Reynolds number for flow over a single cylinder. Mandhani et al. [9] used a numerical model to extract results for the local heat transfer characteristics of the flow over a circular tube bundle for a wide range of Prandtl number. Bouris et al. [10] and Horvat et al. [11] investigated the effect of the tube shape on heat exchange mechanism where they concluded that the elliptic tubes are more efficient. For the optimization of the thermal performance of a tube bundle heat exchanger, numerical studies were performed by Matos et al. [12,13,14] by changing the spacing and the eccentricity of the tubes. Similar investigations were performed by Stanesku et al. [15] and showed that the optimal spacing decreases as the Reynolds number increases and as the length of the heat exchanger in flow direction increases.

As far as the macroscopic porous modeling is concerned, Horvat and Catton [16] used a volume-averaging technique to model the heat transfer of a plate with circular fins.

In all previous works, the heat transfer performance of the heat exchanger was mainly described by the Nusselt number of the flow inside the heat exchanger. Thus, a similar approach was followed in the present work and the heat transfer performance of the heat

exchanger was investigated with the analysis of the overall and local Nusselt numbers and the temperature distributions inside the heat exchanger

2. Description of the flow field inside tube bundles.

For the determination of the phenomena that governs the flow, experimental investigations were performed in wind tunnels where staggered tube bundle heat exchanger cores were mounted. The studies of Umeda and Yang [17] were focused on that direction. In their work an effort was made to derive correlations between the heat exchanger core characteristics and the type of the flow: laminar, turbulent or transitional.

The characteristic Reynolds number of the flow was defined as:

$\mathrm{Re} = \frac{U_{\max} L}{\nu}$, where L is a characteristic length and $U_{\max}$ is the maximum velocity inside the heat exchanger core.

Based on this definition and using the tube diameter as the characteristic length, the flow is considered to be laminar when $\mathrm{Re} < 200$, turbulent when $\mathrm{Re} > 6000$ and transitional when $200 < \mathrm{Re} < 6000$.

Under certain conditions, flow separation can occur downstream the heat exchanger tubes and von Karman vortices are created which are shedding downstream. The

dimensionless number that characterizes such a flow is the Strouhal number as defined in eq. 1:

$$St = \frac{f \cdot D}{U_\infty} \tag{1}$$

where f is the frequency of the shedding vortices and D is the cylinder diameter. The characteristic Reynolds number for a cylinder is defined in eq. 2:

$$\mathrm{Re} = \frac{U_\infty D}{\nu} \tag{2}$$

For Reynolds number values greater than 1000, the Strouhal number of a single cylinder has an almost constant value of 0.21.

Fig. 2 Flow inside a cylinder array

For compact type heat exchangers the spacing between the tubes is characteristically small in order to achieve higher values of heat exchange surface and heat transfer coefficients. In such cases, the flow field development inside the heat exchanger core is being significantly affected by the main flow surrounding the tubes and an 'X-type' flow is being developed, as presented in **Fig. 2**. This type of flow is surrounding the tubes and their wake regions, which remain almost completely stabilized near the trailing edge region of the tubes. However, at the last row of tubes the development of

the wake region is not being limited by the 'X-type' flow and vortex shedding appears and the flow field develops an unsteady nature.

3. Experimental setup

The heat exchanger model is corresponding to the straight part of the complete heat exchanger geometry. It is constructed in a 1:1 scale and consists of 144 elliptic tubes, placed in a 4-3-4 staggered arrangement. Additional details can be found in the work of Albanakis et al. [2]

For the experimental measurements, the air inlet temperature was set at 60°C and 80°C while the air temperature difference between inlet and outlet was equal to ΔT=29°C and ΔT=47°C respectively. For each temperature difference three different flow rates were examined. For the experimental measurements, the corresponding Reynolds numbers indicate that the flow is within the transitional regime. However, as it was shown in the work Missirlis et al. [4,5] a turbulent flow CFD computation can provide useful results.

4. Numerical methodology

The numerical analysis consists of two approaches. In the first approach, the detailed modeling of a characteristic flow passage of the exact geometry of the heat exchanger is performed, as shown in **Fig. 3**. In the second one, the heat exchanger is modeled macroscopically as a porous medium.

As already mentioned, the heat exchanger under investigation consists of a number of elliptic tubes placed in a staggered arrangement. Thus, vortex shedding is expected to appear downstream of the last row of tubes and thus, it was decided to proceed with unsteady computations.

4.1 CFD modeling of a flow passage of the heat exchanger

Fig. 3 Heat exchanger cross section

For the detailed modeling of the heat exchanger an in-house code developed in the Laboratory of Fluid Mechanics and Turbomachinery (*LFMT)* was used. The computational domain consists of one characteristic flow passage, presented in **Fig. 3**.

Even though the computation was performed with a 3D solver, only one plane of the flow was computed, corresponding to the symmetry axis of the wind tunnel. Thus, the flow field solution is performed under a 2D approach.

Thus, a computational grid of 45584 (814×2×156) cells was created. During the grid creation process, special care was given to the regions where significant variations in the flow quantities were expected, as presented in **Fig. 3**.

The boundary conditions that were used are periodicity at the top and bottom boundaries and symmetry in the north - south direction, as presented in **Fig. 3**. In addition, a constant temperature value is imposed on the tube walls, set equal to the temperature of water circulating inside the tubes during the experimental measurements.

Since the flow field is an unsteady one, it was necessary to make an estimation of the time period and the frequency of the vortex shedding behind the elliptic tubes.

Considering that the Strouhal number in shedding flows over a cylinder has a value of 0.21 and using the small axis of the elliptic tube as the characteristic length and the inlet velocity as a characteristic velocity, a frequency of approximately 1000 Hz is calculated and the estimated time period of the vortex shedding is 0.001 sec. Hence, the time step for the unsteady calculation was selected as a small part of the time period and more specifically, equal to1×10^{-5} sec.

The solved equations are the continuity equation, eq. 3, the Favre averaged Navier-Stokes equations, eq. 4, and the equation of energy , eq. 5. For the pressure calculation the SIMPLE algorithm is applied. The density fluctuations calculation was based on the Karki-Patankar [19] procedure. The flow was solved with the Finite Volume Method while the discretization scheme HLPA of Zhu [20] was used. The computation was performed on a cluster of 22 processors, the communication of which was based on MPI.

For the turbulence modeling, eq.6 and eq. 7, the Launder-Sharma low Reynolds k - ε model [21] was used.

Continuity :

$$\frac{\partial \overline{\rho}}{\partial t}+\frac{\partial}{\partial x_i}\left(\overline{\rho}\tilde{u}_i\right)=0 \tag{3}$$

Momentum :

$$\frac{\partial}{\partial t}\left(\overline{\rho}\tilde{u}_i\right)+\frac{\partial}{\partial x_j}\left(\overline{\rho}\tilde{u}_j\tilde{u}_i\right)=-\frac{\partial \overline{p}}{\partial x_i}+\frac{\partial}{\partial x_j}\left(\tilde{\tau}_{ji}^{tot}\right) \tag{4}$$

Total energy :

$$\frac{\partial}{\partial t}\left(\overline{\rho}\tilde{e}_0\right)+\frac{\partial}{\partial x_j}\left(\overline{\rho}\tilde{u}_j\tilde{e}_0+\tilde{u}_j\overline{p}+\tilde{q}_j^{tot}-\tilde{u}_i\tilde{\tau}_{ij}^{tot}\right)=0 \tag{5}$$

where

$$\tilde{e}_0=\tilde{e}+\frac{\tilde{u}_k\tilde{u}_k}{2}+\tilde{k}\ ,\ \tilde{e}=C_v\tilde{T}$$

$$\tilde{\tau}_{ij}^{tot}=\tilde{\tau}_{ij}^{lam}+\tilde{\tau}_{ij}^{turb}$$

$$\tilde{\tau}_{ij}^{lam}=\mu\left(\frac{\partial\tilde{u}_i}{\partial x_j}+\frac{\partial\tilde{u}_j}{\partial x_i}-\frac{2}{3}\frac{\partial\tilde{u}_k}{\partial x_k}\delta_{ij}\right)$$

$$\tilde{\tau}_{ij}^{turb}=\mu_t\left(\frac{\partial\tilde{u}_i}{\partial x_j}+\frac{\partial\tilde{u}_j}{\partial x_i}-\frac{2}{3}\frac{\partial\tilde{u}_k}{\partial x_k}\delta_{ij}\right)-\frac{2}{3}\overline{\rho}\tilde{k}\delta_{ij}$$

$$\tilde{q}_j^{tot}=\tilde{q}_j^{lam}+\tilde{q}_j^{turb}$$

$$\tilde{q}_j^{lam}=-C_p\frac{\mu}{\mathrm{Pr}}\frac{\partial\tilde{T}}{\partial x_j}\ ,\ \tilde{q}_j^{turb}=-C_p\frac{\mu_t}{\mathrm{Pr}_t}\frac{\partial\tilde{T}}{\partial x_j}$$

Turbulence kinetic energy :

$$\frac{\partial\left(\bar{\rho}\tilde{k}\right)}{\partial t}+\frac{\partial}{\partial x_j}\left(\bar{\rho}\tilde{u}_j\tilde{k}\right)=\frac{\partial}{\partial x_j}\left[\left(\mu+\frac{\mu_t}{\sigma_k}\right)\frac{\partial\tilde{k}}{\partial x_j}\right]+P_k-\bar{\rho}\left(\tilde{\varepsilon}^*+2\frac{\mu}{\bar{\rho}}\left(\frac{\partial\sqrt{\tilde{k}}}{\partial x_j}\right)^2\right) \quad (6)$$

where

$$P_k=\tilde{\tau}_{ij}^{turb}\frac{\partial\tilde{u}_i}{\partial x_j}\ ,\ \mu_t=c_\mu f_\mu\bar{\rho}\frac{\tilde{k}^2}{\tilde{\varepsilon}^*}\ ,$$

Isotropic part of turbulent dissipation :

$$\frac{\partial\left(\bar{\rho}\tilde{\varepsilon}^*\right)}{\partial t}+\frac{\partial}{\partial x_j}\left(\bar{\rho}\tilde{u}_j\tilde{\varepsilon}^*\right)=\frac{\partial}{\partial x_j}\left[\left(\mu+\frac{\mu_t}{\sigma_\varepsilon}\right)\frac{\partial\tilde{\varepsilon}^*}{\partial x_j}\right]+c_{\varepsilon1}f_1\bar{\rho}\frac{\tilde{\varepsilon}^*}{\tilde{k}}P_k-c_{\varepsilon2}f_2\bar{\rho}\frac{\tilde{\varepsilon}^{*2}}{\tilde{k}}+2\mu_t\frac{\mu}{\bar{\rho}}\left(\frac{\partial^2\tilde{u}_i}{\partial x_j\partial x_k}\right)^2 \quad (7)$$

where

$$f_\mu=\exp\left(\frac{-3.4}{\left(1+R_T/50\right)^2}\right)\ ,\ f_1=1\ ,\ f_2=1-0.3\exp\left(-R_T^2\right)\ ,\ R_T=\frac{\bar{\rho}\tilde{k}^2}{\mu\tilde{\varepsilon}^*}\ ,$$

$c_{\varepsilon1}=1.44$, $c_{\varepsilon2}=1.92$, $c_\mu=0.09$, $\sigma_k=1.0$, $\sigma_\varepsilon=1.3$

The dynamic viscosity μ is considered to be temperature dependent following the Sutherland's law:

$\mu = \mu_0 \left(\frac{\tilde{T}}{T_0} \right)^{3/2} \left(\frac{T_0 + C}{\tilde{T} + C} \right)$, where the reference values are

$\mu_0 = 1.716 \cdot 10^{-5}\, Pa \cdot s$, $T_0 = 273.15\, K$ and $C = 110.6$.

4.2 Porous medium modeling of the heat exchanger

In this approach, the presence of the heat exchanger was modelled as a porous medium with predefined pressure drop and heat transfer behaviour.

For the pressure drop the modified form of the Darcy-Forchheimmer law, presented in Yakinthos et al. [22], was used. As presented in eq. 8:

$$S_M = D'V + \frac{1}{2} F' \left| \vec{V} \right| V$$

$$S_M = \begin{pmatrix} \partial p / \partial x \\ \partial p / \partial y \\ \partial p / \partial z \end{pmatrix},\ V = \begin{pmatrix} u \\ v \\ w \end{pmatrix},\ D' = \begin{pmatrix} D'_{xx} & D'_{xy} & D'_{xz} \\ D'_{yx} & D'_{yy} & D'_{yz} \\ D'_{zx} & D'_{zy} & D'_{zz} \end{pmatrix},\ F' = \begin{pmatrix} F'_{xx} & F'_{xy} & F'_{xz} \\ F'_{yx} & F'_{yy} & F'_{yz} \\ F'_{zx} & F'_{zy} & F'_{zz} \end{pmatrix} \quad (8)$$

The pressure drop terms have been adopted in the flow calculation as source terms in the momentum equations.

At the next step, in order to include the heat transfer effect, it was necessary to incorporate a heat transfer model. Towards this direction and based on the conclusions

of a literature survey of Zukauskas [23], it was decided to follow an approach based on the Nusselt number.

Thus, a correlation for the total Nusselt number of the heat exchanger was derived from the experimental data as a function of Prandtl and Reynolds numbers as presented in eq. 9:

$$Nu = a\,\mathrm{Pr}^{b}\,\mathrm{Re}^{c} \tag{9}$$

where $\mathrm{Re} = \dfrac{\rho \bar{u} D_h}{\mu}$

$\bar{u}$ the average axial velocity and the values of coefficients *a*, *b* and *c* were derived from the experimental measurements through a curve fitting process.

At the next step, the heat transfer coefficient *h* can be estimated using the definition of the Nusselt number, eq. 10:

$$Nu = \frac{hD_h}{\kappa} \tag{10}$$

where D_h is the equivalent diameter of the elliptic tube of the heat exchanger.

When a porous medium modeling is attempted it is necessary to compute a local heat transfer coefficient in the regions of the heat exchanger. For this reason, the

experimentally derived Nusselt-Prandtl-Reynolds correlation was applied in the computational model in the regions of the heat exchanger.

Hence, a local heat transfer coefficient h_{local} is estimated using a local Reynolds, as:

$$\mathrm{Re} = \frac{\rho u D_h}{\mu}$$

where u is the local flow velocity.

At last, the heat source term, which is included in the energy equation, is calculated as presented in eq. 11:

$$\dot{q} = h_{local} A \left(T_f - T_w \right) \tag{11}$$

where

$\dot{q}$ is the heat flux per unit volume

A is the heat exchange surface per unit of volume

T_f is the local fluid temperature

T_w is the water temperature during the experimental measurements

At the next stage, a computational grid of 17024 (266×1×64) computational cells was created as presented in **Fig. 4**. This time the computational domain includes the overall heat exchanger model mounted inside the wind tunnel. At the region occupied by the heat exchanger, the pressure drop and heat transfer laws were applied.

Fig. 4 Computational domain and grid used in the porous medium modeling (the region of the heat exchanger is indicated with red colour)

For the turbulence modeling the Launder-Sharma low Reynolds k - ε model [21] was used.

The computational domain is presented in **Fig. 4**. As it can be seen the computational grid corresponds to the symmetry 2D plane of the wind tunnel setup.

Regarding the boundary conditions of the computations, at the inlet of the computational domain a uniform velocity profile and the static pressure is applied. The wind tunnel walls are considered as adiabatic. The CFD computations were performed with the use of the 3D in-house academic solver. Thus, since the selected computational domain corresponds to the wind tunnel symmetry plane, symmetry boundary conditions were used in the north - south direction, as presented in **Fig. 4**.

5. Results

For the evaluation of the thermal performance of the heat exchanger, the Nusselt number of the numerical investigation is compared to the one of the experimental measurements. Additionally, in the CFD modeling of the flow passage geometry, both the average and the local Nusselt number are calculated for further analysis of the heat transfer efficiency of the heat exchanger.

The Nusselt number is calculated as, eq. 12:

$$Nu = \frac{hD}{\kappa} \tag{12}$$

where κ is the thermal conductivity of air, with its value being a function of temperature based on the values of thermodynamic tables, eq 13.

$$\kappa = 2.7676 \cdot 10^{-11} T^3 - 6.7098 \cdot 10^{-8} T^2 + 1.0704 \cdot 10^{-4} T - 6.1922 \cdot 10^{-4} \tag{13}$$

For the local Nusselt number the heat transfer coefficient is, eq. 14 :

$$h = \frac{\dot{q}_w}{A \cdot \Delta T} \tag{14}$$

where $\dot{q}_w$ is the wall heat flux and A is the heat exchange surface .

The temperature difference ΔT can be either $\Delta T_m = T_m - T_w$, where T_m is the mean temperature of the heat exchanger, $T_m = \frac{T_{in} + T_{out}}{2}$, used mainly in experimental work, Kurtbas [24], or $\Delta T_b = T_b - T_w$, where T_b is the local bulk temperature, Jang and Yang [25]. The local Nusselt number was calculated by taking into account both definitions of the temperature difference ΔT. The first one for compatibility with the experimental data and the second one for a better understanding of the heat transfer mechanism.

Typical results are presented in **Fig. 5**, for the seven tubes t1 to t7 indicated in **Fig. 3**. The results of the Nusselt number distribution are presented in relation to a characteristic reference value, Nu_{ref}, corresponding to a typical operation condition of the heat exchanger. The distribution of the Nusselt number is presented as a function of non-dimensional arc length along the surface of the elliptical tube. It must be mentioned that for all cases under investigation similar Nusselt number distributions were computed. Thus, for space economy reasons, the results of only two cases are presented corresponding to T_{inlet}= 333K, u=6.5 m/s.

Fig. 5 Distribution of Nusselt for T_{in}=333K calculated a) with T_m and b) with T_b,

As it can be seen, the Nusselt number distribution can be divided into five distinct regions. The first one is located near the leading edge of the elliptic tube and the second one at the elliptic tube side while the last three regions cover the remaining part of the elliptic tube up to its trailing edge. In all cases, the Nusselt number is taking its maximum values near the stagnation point of the elliptic tube and then decreases rapidly until point A, presented in **Fig. 6**, which is corresponding to the point of the maximum flow acceleration near the elliptic tube. From this point and until point B, the Nusselt number is having small variations and an almost constant value. From point B and to point C the Nusselt number begins increasing to a local maximum, which coincides with the point A of the upper tube where the flow is accelerating. Then, there is a small decrease of the Nusselt number due to the recirculation which develops near the trailing edge of the tube, point D, and just after that, another local maximum is presented at the second stagnation point at the trailing edge of the tube.

The maximum local Nusselt number appears at the stagnation point of each tube and the overall maximum is always on the second tube (t2), due to the acceleration of the flow that enters the heat exchanger.

Fig. 6 a**)** Velocity and b)Temperature fleld (T_{in}=333K, u_{in}=6.5 m/s)

In **Fig. 6** typical velocity and temperature distributions between the tubes are shown. The points A and B, C and D are also indicated.

Regarding the flow field development inside the heat exchanger core, the wake of the tubes can be considered as stable since no signs of vortex shedding are presented, **Fig. 7**.

Fig. 7 Streamlines of flow velocity a) inside the heat exchanger core, b) last tube t=T/4, c) last tube t=3T/4

On the other hand, the vortices behind the last tube are shedding.

In order to investigate the possible effect of the unsteady nature of the flow in the heat transfer performance of the heat exchanger, the local Nusselt number fluctuations with time were computed as presented in **Fig. 8**. As can be seen, the flow field unsteadiness

does not seem to affect the heat transfer, as the local Nusselt number presents no significant variations with time. More specifically, in the first six rows (t1-t6), where no vortex shedding is appearing behind the tubes, negligible variations are presented and the Nusselt number has a constant value with time. A small variation is noticed only on the last tube, in the area that is affected by the vortex shedding, as shown in **Fig. 8**.

The frequency of the separation is in the range of 1.02 – 1.35 kHz depending on the inlet flow velocity and it is almost a linear function of velocity.

As a result, the Strouhal number is almost constant $St = \frac{f \cdot L}{u}$.

For the Strouhal number calculation, the small axis of the elliptic tube was chosen as the characteristic length and hence

$$St = \frac{f \cdot 2b}{u_m}$$

where u_m is the mean velocity of the flow.

For all cases under investigation the Strouhal number is equal to $St \approx 0.3$

Fig. 8 Nusselt fluctuation in time

In order to evaluate the heat transfer performance of each tube, the average Nusselt number for all test cases was computed as presented in **Fig. 9**. More specifically, in **Fig. 9a** the average Nusselt number is calculated using the mean inlet – outlet temperature for inlet temperature of 333K. Noticeably, in all cases the first and second tubes have the highest Nusselt number values, with the maximum being presented for the second

tube, while the Nusselt number values are significantly reduced for the rest of the tubes. Additionally, in all diagrams a higher velocity results in higher Nusselt number.

Fig. 9 Nusselt for each tube, T_{in}=333K using a) T_m and b) T_b.

The same conclusions can be derived from the **Fig. 9b**, where the average Nusselt number for each tube is calculated, but this time based on the bulk temperature. The Nusselt number is higher for the first two tubes and it is almost constant after the third tube regardless the inlet flow velocity. This also indicates that the contribution of the two first tubes to total heat exchanger efficiency is significant.

Furthermore, even though the distribution of the average Nusselt number for each tube differs according to the calculation approach, mean or bulk, the total Nusselt number of the heat exchanger calculated for each case using both approaches is almost equal.

In **Fig. 10** there is a comparison of the measured and calculated total Nusselt number (mean) of the heat exchanger. The Nusselt number increases with the velocity in both experimental measurements and computational results. For the comparison, the experimental Nusselt number values were calculated using the same temperature difference definition as the computational results.

Fig. 10 Total Nusselt for T_{in}=333K

In the case of the porous medium approach, the same test cases as in the CFD modeling of the flow passage of the heat exchanger were computed and the results were compared to the experimental measurements.

The computed outlet temperature of the simulations is presented in **Table 1**. It must be mentioned that the experimental value of the outlet temperature is 304K for the case of T_{in}=333K. As it can be seen the CFD results of both approaches are in good agreement with the experimental measurements.

Table 1 Outlet temperature for T_{in}=333K

A comparison of the static pressure drop computed with both CFD approaches and the experimental measurements is shown in **Fig. 11**. The CFD results of the porous medium approach and the experimental measurement are in very good agreement. The results of the CFD modeling of the flow passage of the heat exchanger follow the same trend as the experimental measurements and the results of the porous medium approach, however a relatively constant deviation appears. This difference can be partially attributed to the fact that wind tunnel walls and their effect have not been taken into account in the case of the CFD flow passage modeling where periodic boundary conditions were used.

Fig. 11 Static pressure drop for T_{in}=333K

6. Conclusions

In the present work, the heat transfer performance of a heat exchanger designed for aero engine applications was investigated. The investigation was performed with the use of two CFD approaches, the first one with full modeling of a flow passage of the exact geometry of the heat exchanger and the second one considering the heat exchanger as a porous medium with predefined heat transfer and pressure drop behaviour. The numerical results of both approaches concerning the heat transfer and the temperature distribution were compared with experimental data and with each other and were found to be in good agreement. The thermal behaviour of the heat exchanger core was performed using an analysis based on the local Nusselt number. The thermal investigation of the heat exchanger revealed that the first and second tubes have a significant role in the total thermal efficiency of the heat exchanger as can be seen by the Nusselt number distribution. Moreover, the effect of the unsteady nature of the flow field in the last row of the heat exchanger tubes was examined and shown to have a limited effect on the total heat transfer performance of the heat exchanger.

Acknowledgements

This paper is part of the 03ED research project, implemented within the framework of the ‘‘Reinforcement Programme of Human Research Manpower” (PENED) and co-financed by National and Community Funds 25% from the Greek Ministry of Development-General Secretariat of Research and Technology and 75% from E.U. –

European Social Fund. A part of this project has been also funded by MTU Aero Engines GmbH.

References

[1] S. Boggia and K. Rüd, Intercooled recuperated aero engine, Technical report, Advanced Project Design, MTU Aero Engines Munchen, Germany, 2004.

[2] C. Albanakis, K.Yakinthos, K. Kritikos, D. Missirlis, A. Goulas and P. Storm, The effect of heat transfer on the pressure drop through a heat exchanger for aero engine applications, Applied Thermal Engineering 29 (2009) 634-644.

[3] D. Missirlis, K. Yakinthos, A. Palikaras, K. Katheder and A. Goulas, Experimental and numerical investigation of the flow field through a heat exchanger for aero-engine applications, International Journal of Heat and Fluid Flow 26 (2005) 440-458.

[4] D. Missirlis, K. Yakinthos, P. Storm and A. Goulas, Modeling pressure drop of inclined flow through a heat exchanger for aero-engine applications, International Journal of Heat and Fluid Flow 28 (2007) 512-515.

[5] K. Yakinthos, D. Missirlis, A. Palikaras, and A. Goulas, Heat Exchangers for Aero Engine Applications, ASME Conference Proceedings 2006:47845 (2006) 653-662.

[6] K. Yakinthos, , D. Missirlis, A. Palikaras, P. Storm, B. Simon, and A. Goulas, Optimization of the design of recuperative heat exchangers in the exhaust nozzle of an aero engine, Applied Mathematical Modelling 31 (2007) 2524-2541.

[7] A. Zukauskas and R. Ulinskas, Efficiency Parameters for Heat Transfer in Tube Banks, Heat Transfer Engineering 6:1 (1985) 19 – 25.

[8] R. A. Ahmad, Steady-State Numerical Solution of the Navier-Stokes and Energy Equations around a Horizontal Cylinder at Moderate Reynolds Numbers from 100 to

500, Heat Transfer Engineering 17:1 (1996) 31-81.

[9] V. K. Mandhani, R. P. Chhabra and V. Eswaran, Forced convection heat transfer in tube banks in cross flow, Chemical Engineering Science 57 (2002) 379-391.

[10] D. Bouris, G. Papadakis and G. Bergeles, Numerical evaluation of alternate tube configurations for particle deposition rate reduction in heat exchanger tube bundles, International Journal of Heat and Fluid Flow 22 (2001) 525-536.

[11] A. Horvat, M.Leskovar and B. Mavko, Comparison of heat transfer conditions in tube bundle cross-flow for different tube shapes, International Journal of Heat and Mass Transfer 49 (2006) 1027-1038.

[12] R. Matos, J. Vargas and T. Laursen, Optimization study and heat transfer comparison of staggered circular and elliptic tubes in forced convection, International Journal of Heat and Mass Transfer 44 (2001) 3953-3961.

[13] R. Matos, T. Laursen, J. Vargas and A. Bejan, Three-dimensional optimization of staggered finned circular and elliptic tubes in forced convection, International Journal of Thermal Sciences 43 (2004) 477-487.

[14] R. Matos, J. Vargas and T. Laursen, Optimally staggered finned circular and elliptic tubes in forced convection, International Journal of Heat and Mass Transfer 47 (2004) 1347-1359.

[15] G. Stanescu, A. J. Fowler and A. Bejan, The optimal spacing of cylinders in free-stream cross-flow forced convection, Int. J. Heat Mass Transfer 39:2 (1996) 311-317.

[16] A. Horvat and I. Catton, Numerical technique for modeling conjugate heat transfer in an electronic device heat sink, International Journal of Heat and Mass Transfer 46 (2003) 2155-2168.

[17] S. Umeda and W. Yang, Interaction of von Karman vortices and intersecting main

streams in staggered tube bundles, Experiments in Fluids 26 (1999) 389-396.

[18] K. C. Karki and S. V. Patankar, Pressure Based Calculation Procedure for Viscous Flows at All Speeds in Arbitrary Configurations, AIAA JOURNAL 27:9 (1989) 1167-1174.

[19] J. Zhu, A low-diffusive and oscillation-free convection scheme , Communications in Applied Numerical Methods 7:3 (1991) 225-232.

[20] B. Launder and B. Sharma, Application of the energy-dissipation model of turbulence to the calculation of flow near a spinning disc, Letters In Heat And Mass Transfer 1 (1974) 131-138.

[21] K. Yakinthos, S. Donnerhack, D. Missirlis, O. Seite, and P. Storm, Derivation of an anisotropic model for the pressure loss through a heat exchanger for aero engine applications, (GT2009), Proceedings of ASME Turbo Expo 2009: Power for Land, Sea and Air', Orlando, Florida, USA, 2009.

[22] I. Kurtbaş, The effect of different inlet conditions of air in a rectangular channel on convection heat transfer: Turbulence flow, Experimental Thermal and Fluid Science 33 (2008) 140-152.

[23] J. Jang and J. Yang, Experimental and 3-D Numerical Analysis of the Thermal-Hydraulic Characteristics of Elliptic Finned-Tube Heat Exchangers, Heat Transfer Engineering 19:4 (1998) 55-67.

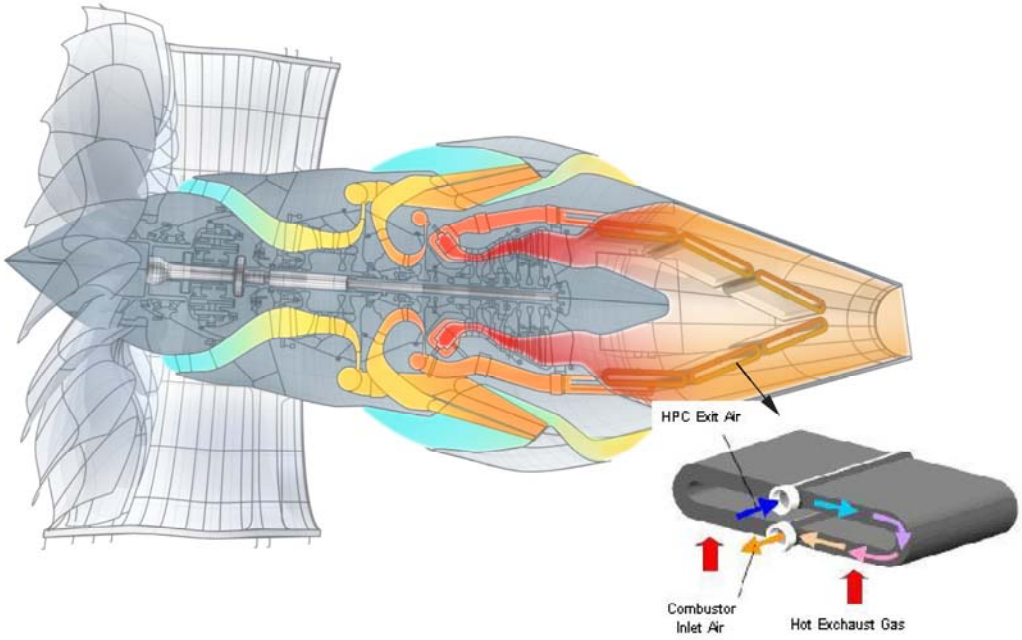

Figure 1. The IRA aero engine

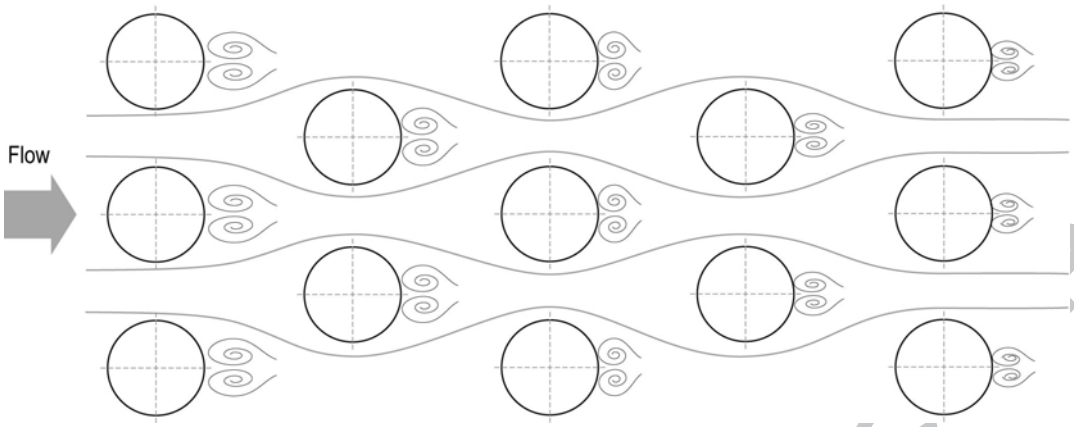

Figure 2. Flow inside a cylinder array

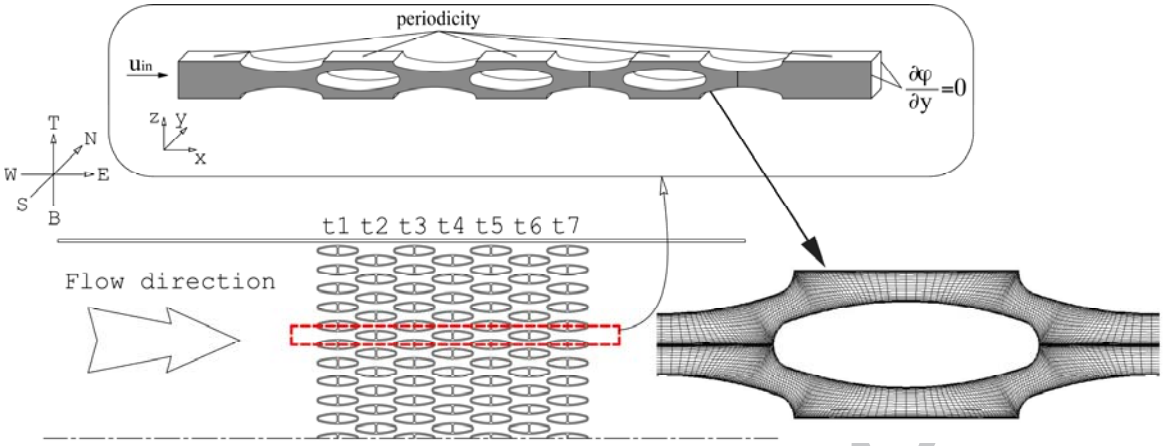

Figure 3. Heat exchanger cross section

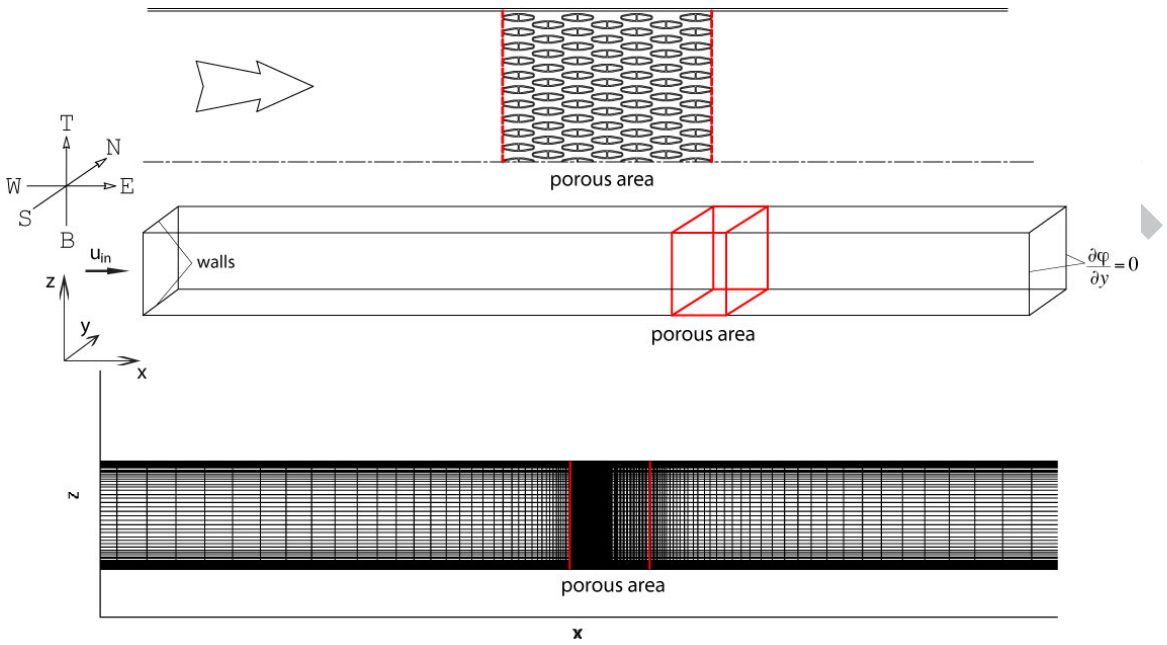

Figure 4. Computational domain and grid used in the porous medium modeling (the region of the heat exchanger is indicated with red colour)

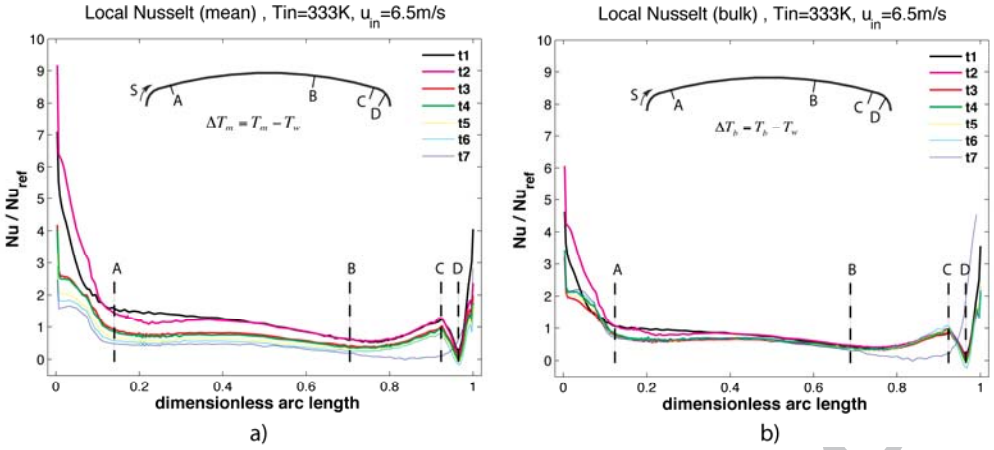

Figure 5. Distribution of Nusselt for T_{in}=333K calculated a) with T_m and b) with T_b,

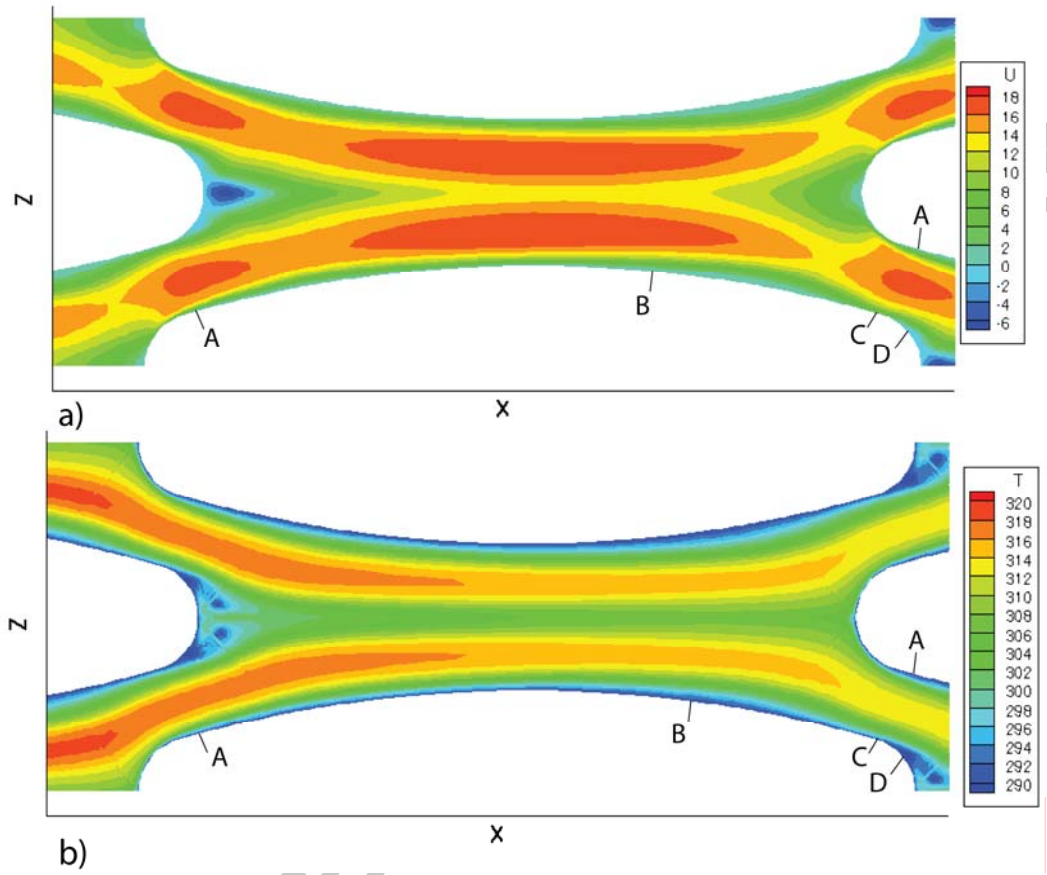

Figure 6. a)Velocity and b) Temperature field (T_{in}=333K, u_{in}=6.5 m/s)

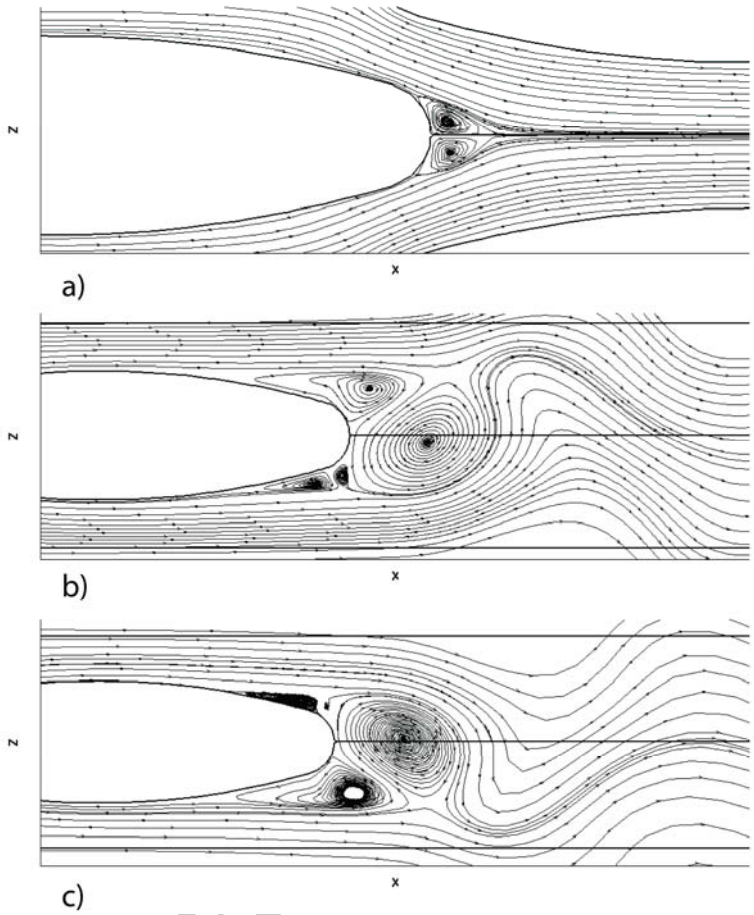

Figure 7. Streamlines of flow velocity a) inside the heat exchanger core, b) last tube t=T/4, c) last tube t=3T/4

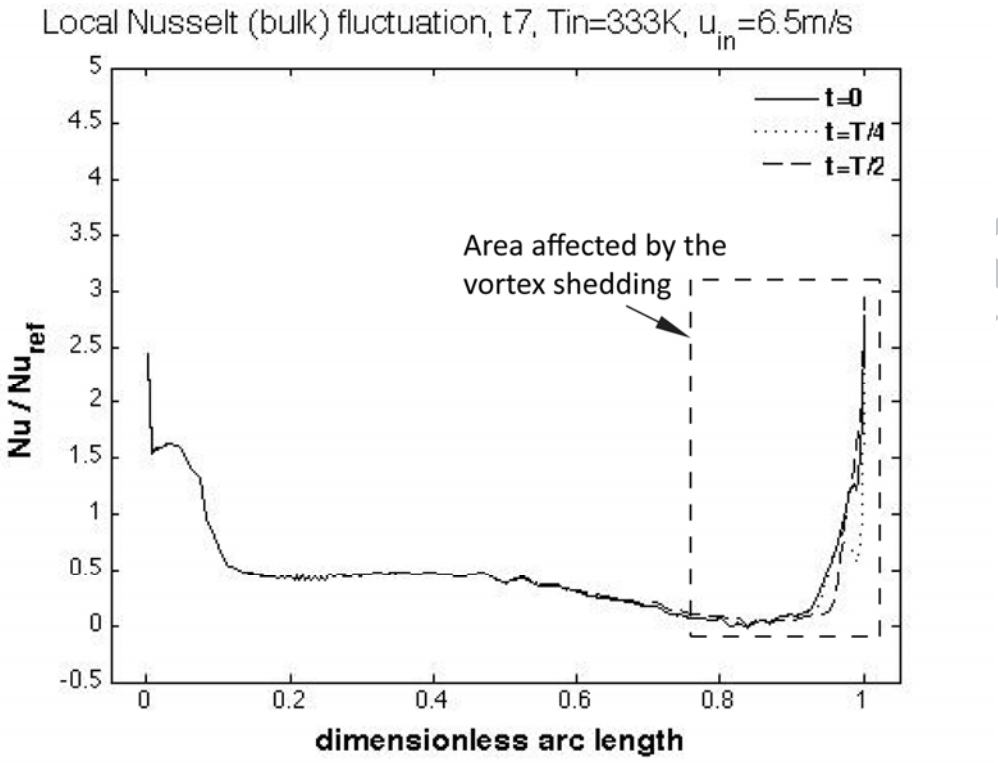

Figure 8. Nusselt fluctuation in time

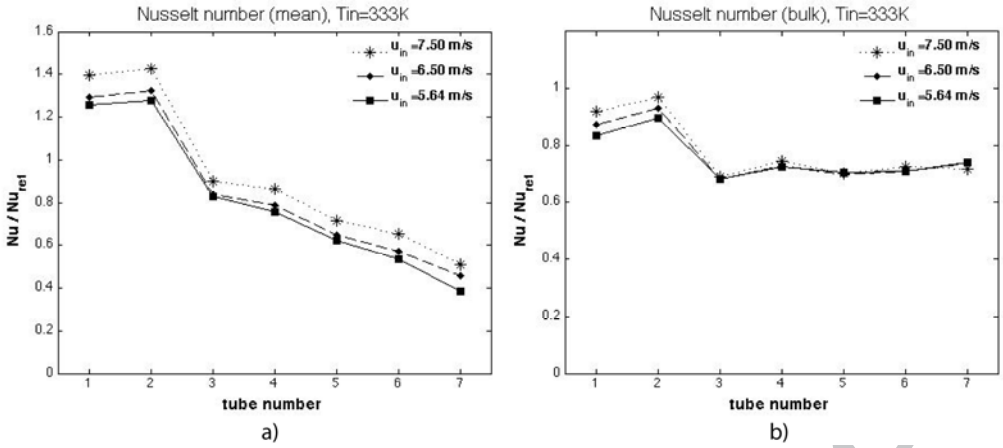

Figure 9. Average Nusselt for each tube, T_{in}=333K using a) T_m and b) T_b.

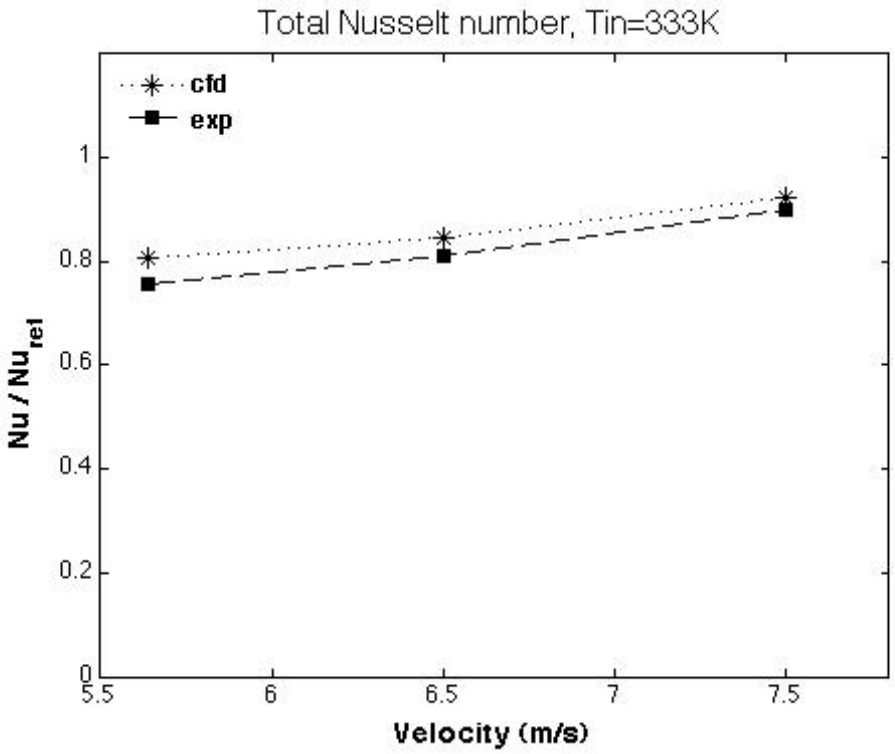

Figure 10. Total Nusselt for T_{in}=333K

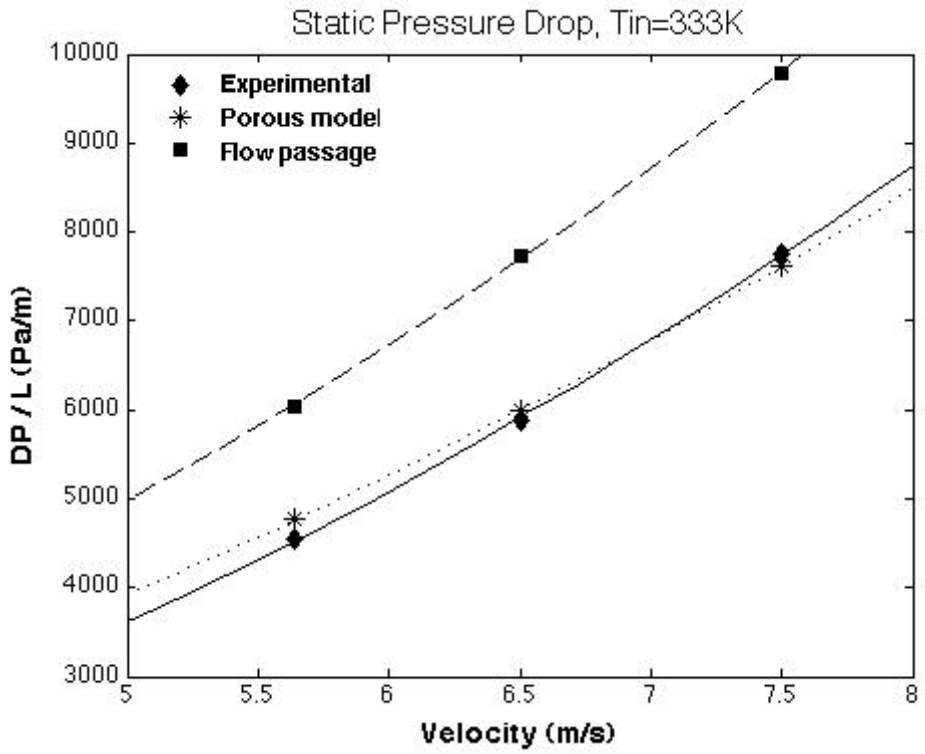

Figure 11. Static pressure drop for T_{in}=333K

	T_{out} (K) for T_{in}=333K	
u_{in} (m/s)	Cfd porous	cfd 1:1
7.51	304.90	305.50
6.50	304.60	305.00
5.64	304.40	304.38

Table 1. Outlet temperature for T_{in}=333K